Annual Report 2023 JMBC – Research Highlight

This highlight refers to the PhD by Martin van der Eijk (2023, cum laude)

Slamming of structures on aerated water

Martin van der Eijk and Peter Wellens
Delft University of Technology, Mechanical Engineering, Ship Hydromechanics

Background

Maritime structures in heavy seas can experience wave impact events with high loads. Impact events can be influenced by the presence of air in water through compressibility (Bredmose et al., 2009; Za et al., 2016; Plumerault et al., 2012). Compressibility leads to lower impact pressures and the generation of high-frequency load variations due to density waves. Quantification of the influence of aeration on impact pressures through numerical methods was challenging before.

A new cartesian grid method, an extension of our work (van der Eijk & Wellens, 2019, 2023, 2024) for compressible multiphase flow, is introduced to account for water, air and homogeneous mixtures of air and water. The method is designed to predict the hydrodynamic loads on moving bodies engaging with interfaces between fluids having large density ratios. An equation for conservation of energy is omitted by enforcing pressure-density relations.

New experimental data of 2D wedge impacts with aerated water, made available as open data, are presented to demonstrate the validity of the numerical method.

Method

Computing the position of the fluid-fluid and the fluid-body interfaces accurately is relevant for determining the moment of impact. A colour function $f(x,t)$ is used to capture the position of the interface. Transport of the interface is described by

$$\frac{Df}{Dt} = \frac{\partial f}{\partial t} + (\mathbf{u} \,.\, \boldsymbol{\nabla}) f = 0, \tag{1}$$

in which $f(x,t) = 0$ gives the position of the interface and $\mathbf{u}$ the interface velocity. Eq. (1) is implemented as a Volume-of-Fluid algorithm.

The positions of the interfaces lead to volume fractions. The definition of the volume fractions is given in Figure 1. Volume fraction C_b indicates the part of a volume that is open to fluid. Fraction (1−C_b) then represents the part of a volume that is occupied by a (moving) body. Volume fraction C_a indicates the part of a volume that is occupied with gas (air), where C_f gives the part of the volume occupied with liquid, either water or aerated water, a homogeneous mixture of air and water.

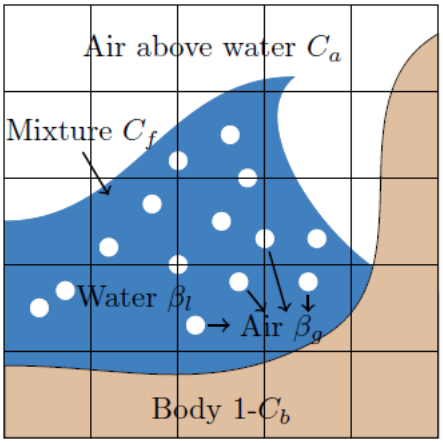

Figure 1: Illustration of the phases of matter in the solver and how they are represented discretely in the cartesian grid. Volume fraction C_f is used for representing aerated water, C_a for air above the water, β_l for the water part of the homogeneous air-water mixture, β_g for the air part. C_b gives the part of a volume not occupied by the body and open to fluid.

Following Plumerault et al. (2012), additional volume fraction fields are introduced to indicate the part by volume of the homogeneous mixture that is gas, β_g, and the part that is water, β_l. These volume fractions are necessary for the formulation of the mathematical model. The governing equations are formulated for a multiphase flow of immiscible Newtonian fluids. An equation for the conservation of mass, using a single velocity field $\mathbf{u}$, is formulated for each phase

$$\frac{\partial \alpha_k \rho_k}{\partial t} + \boldsymbol{\nabla} . (\alpha_k \rho_k \, \mathbf{u}) = 0, \quad k = a, l, g \tag{2}$$

in which subscript a stands for air above water, l for the liquid part of the phase with aerated water, and g for the air part of the aerated water phase. Fractions α_k are defined as

$$\alpha_a = \frac{C_a}{C_b}, \qquad \alpha_l = \frac{\beta_l C_f}{C_b}, \qquad \alpha_g = \frac{\beta_g C_f}{C_b} \tag{3}$$

Using ρ as the density of the aggregate fluid, the equations for the conservation of momentum read

$$\frac{\partial \rho \mathbf{u}}{\partial t} + \boldsymbol{\nabla} . (\rho \mathbf{u} \otimes \mathbf{u}) + \boldsymbol{\nabla} p + \rho \mathbf{g} = 0. \tag{4}$$

Here, p is the pressure in the aggregate fluid and $\mathbf{g}$ the vector of the acceleration of gravity. Note that the viscous term has been omitted from the momentum equation as mainly short-duration events will be considered, in which viscous effects such as the formation of boundary layers can be ignored.

The governing equations require closure that for reasons of efficiency is not obtained through solving an energy relation, but by means of a formulation for the speed of sound of the mixture. For the air-water mixture we define a mixture density (ρ_f) as follows

$$\rho_f = (1 - \beta_g)\rho_l + \beta_g \rho_a, \qquad \rho = \frac{C_f}{C_b}\rho_f + \frac{C_b - C_f}{C_b}\rho_a. \tag{5}$$

According to the equation of Wood (1941), rewritten by making use of the volume fractions of the different phases, the speed of sound formulation for homogeneous mixtures becomes

$$\frac{1}{\rho c^2} = \frac{\frac{c_{b-}\, c_f}{c_b}}{\rho_a c_a^2} + \frac{\frac{c_f}{c_b}}{\rho_f c_f^2} \tag{6}$$

This mixture speed of sound c_f (Wood, 1941) is illustrated in Figure 2; it shows a large decrease in speed of sound for a small fraction of β_g, even up to values lower than the speed of sound of air c_a and water c_l at atmospheric conditions. The low speed of sound explains the relevance of compressibility (Mach number) for aerated impacts.

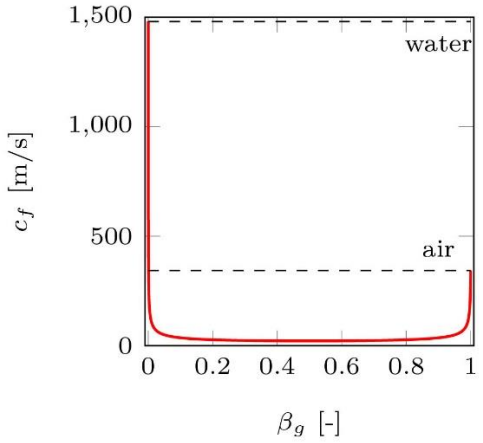

Figure 2: Woods' formulation in Eq. (6) for mixture sound of speed c_f Plotted for air volume fraction β_g assuming C_f = 1.

Results

The test case with a shock bubble is performed to investigate how density waves change direction and how they are transmitted between fluids in simulations with a compressible multiphase method. Helium shock-bubble experiments were performed by Haas and Sturtevant (1987) and the results serve as a benchmark.

The simulation setup for the 2D helium shock bubble case is illustrated in Figure 3. Air, initially, is in two states on either side of the domain. A cylindrical helium bubble is placed in the air at one of these states, approximately in the middle of the domain. The domain boundaries are closed with atmospheric pressure prescribed on the left horizontal end of the domain.

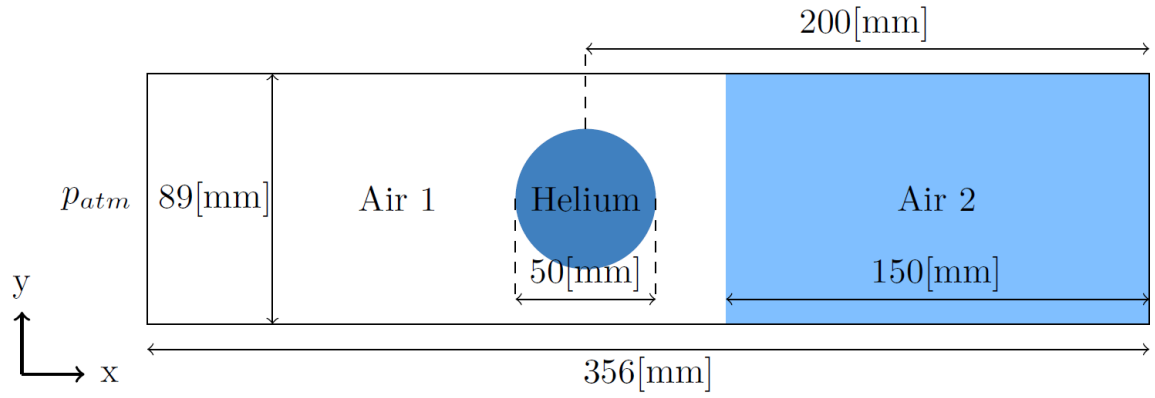

Figure 3: Shock bubble: simulation setup with air at two states of pressure, and helium bubble in the air at one of these states.

Quirk and Karni (1996) conducted a detailed numerical study of the helium shock bubble. Kreeft and Koren (2010) also simulated the shock bubble, but with different fluid properties using a density-based model solving Kapila's five-equation model for inviscid, non-heat-conducting, compressible two-fluid flows.

In our simulations, the front of the density wave before interacting with the helium bubble at t =0 [s], is smeared out over ten grid cells. We chose the position in the middle of these 10 cells as the position of the density wave front to compare with the results from literature. The results of the simulations are given in terms of the positions and the velocities of the interfaces and the density wave fronts. The definition of all interfaces and shock fronts is given in Figure 4a. Interfaces and shock fronts are identified by their velocities v. Figure 4b features a space-time plot of the interfaces, in which the results of the numerical method at three grid resolutions is compared with the results of Quirk and Karni [6]. The positions of the interfaces over time are in good agreement with Quirk and Karni (1996).

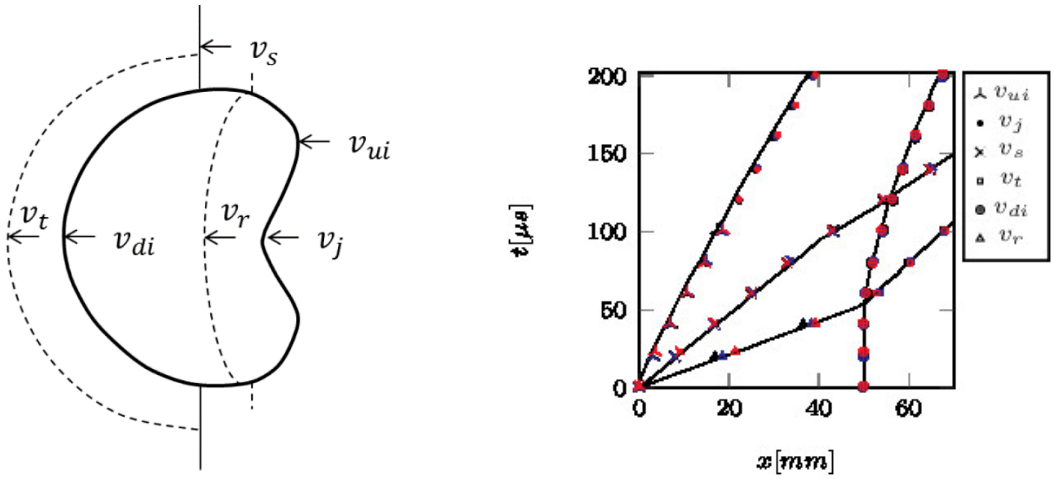

(a) Definition of interfaces and density wave fronts. *(b) Space-time plot of interface positions.*

Figure 4. Shock bubble: definition of interfaces and density wave fronts together with a space time plot of the position of the interfaces and wave fronts. Numerical results (markers) at three grid resolutions: 400x50 (black symbols), 800x100 (blue symbols) and 1200x150 (red symbols), compared with Quirk and Karni (1996) (solid lines).

Experiments for impacts with aeration are rare. Trying to avoid the effect of cavitation, encountered by Ma et al. (2016), because our numerical method would not be able to deal with it, we chose to conduct an experiment with falling wedges.

The setup of the experiment consists of three parts: a box containing aerated water, a fall tower and a wedge attached to a guiding mechanism within the fall tower. The fall height from the tip of the wedge to the initial free surface of the water is at most 2.83 [m] so that, with friction, a maximum impact speed V_i up to 7.0 [m/s] can be achieved. The box and wedge are illustrated in Figure 5, in which α is the deadrise angle.

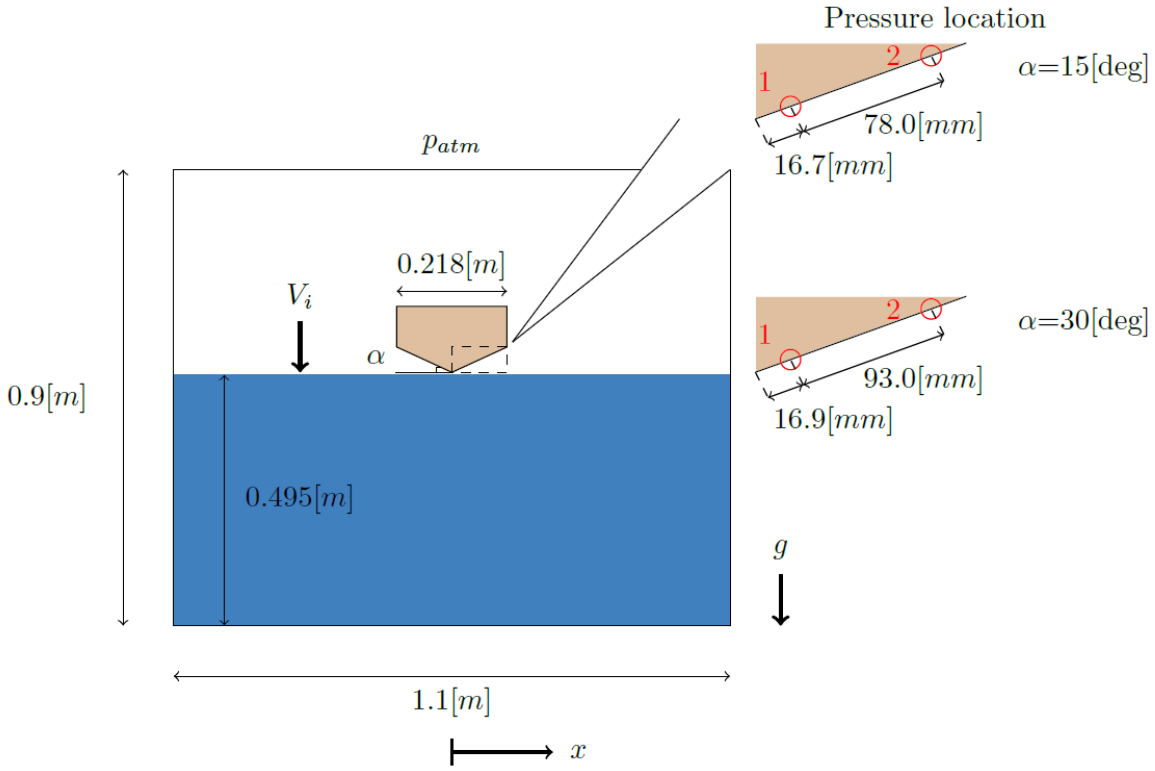

Figure 5: Setup of wedge impact experiment with aerated water. Dimensions of the experiment are also the dimensions of the numerical domain.

Two wedges are used, each with a mass of 31.78 [kg/m], having different deadrise angles (α). One has a deadrise angle of 15 [deg]; the other with 30 [deg] deadrise angle is not discussed further. Pressure sensors were used at two different locations along the bottom of the wedge to measure the impact.

Air bubbles in water are created at the bottom of the box. The experiment is conducted for four aeration levels (β_g = 0.0, 0.01, 0.02, 0.04 [-]). Figure 6 shows the pressures obtained from the numerical simulations with grid 109x29 together with the pressures obtained from the tests in the experiment. The atmospheric pressure was subtracted from all results. Solid blue lines are for pressure sensor 1 and dashed blue lines are for pressure sensor 2. The blue lines for the pressure from the experiment are the average of ten signals. A band is formed along the lines representing one standard deviation above and below the average. Red lines in Figure 6 represent the pressures from the simulations, solid lines for pressure sensor 1 and dashed lines for pressure sensor 2. The lines are the average pressures

obtained from two simulations- at each aeration level β_g with the minimum and maximum value measured at that level on either side of the wedge.

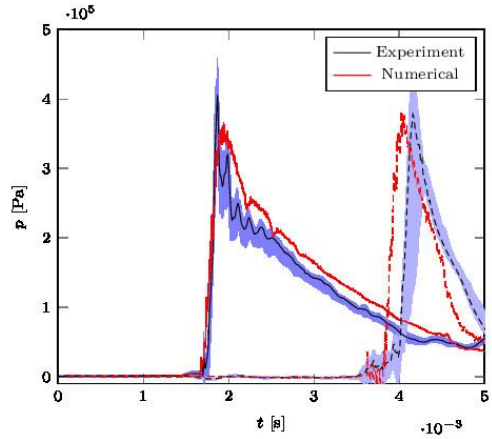

(a) β_g=0.0 [-] and α=15 [deg].

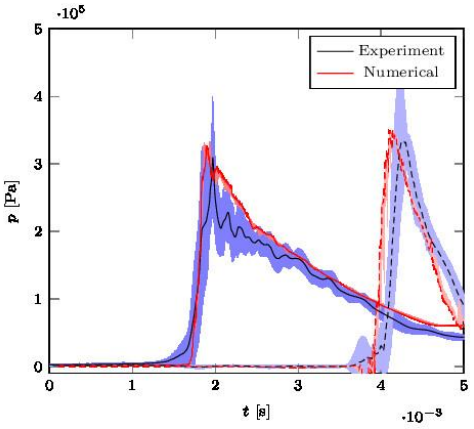

(b) β_g=0.01 [-] and α=15 [deg].

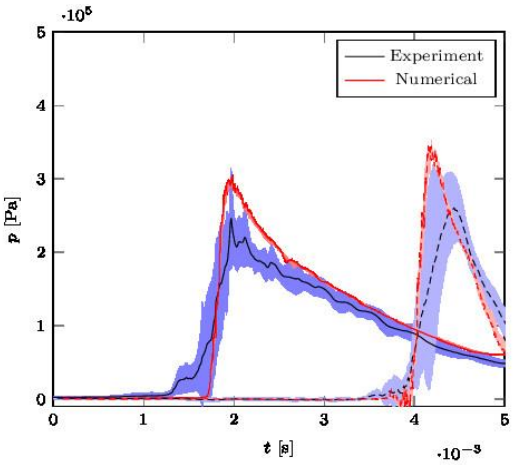

c) β_g=0.02 [-] and α=15 [deg].

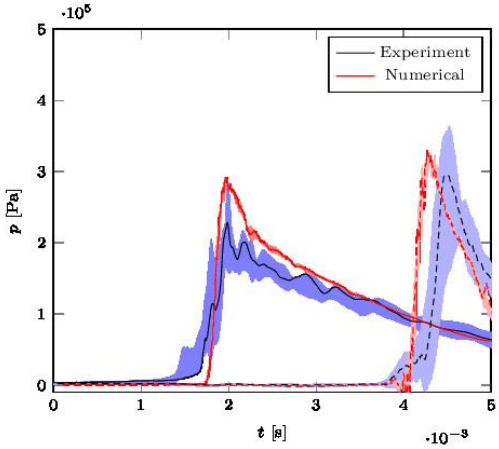

(d) β_g=0.04 [-] and α=15 [deg].

Figure 6. Impact pressures: simulation results (red) with experimental results (blue) for two pressure positions. Pressure sensor 1 is represented by solid lines (__). Pressure sensor 2 is represented by dashed lines (- - -). Band for the experiments composed of one standard deviation below and one above average pressure. Grid 109×29 was used for the simulations. Simulated pressures are the average of two simulations with the minimum and maximum value for aeration at that level. Band around numerical results formed by minimum and maximum. Uncertainty of grid convergence not included in graphs.

The simulated pressures show good agreement with the measured pressures for all aeration levels. The lower aeration levels are represented better than the higher aeration levels; this is thought to be caused by inhomogeneity of the air-water mixture at higher air content, and 3D interaction effects of air bubbles.

The wedge impacting with the aerated water generates density waves due to the compressibility of the air-water mixture. The density waves reflect off of domain boundaries and propagate back to the wedge. The back-and-forth propagation of the density waves causes high-frequency pressure oscillations on the wedge. A time sequence of the simulated pressure after impact for the wedge with

α = 15 [deg] and for aerated water with β_g = 0.04 [-] is shown in Figure 7. The density waves become apparent by their front, which shows as a barrier between regions with higher and lower pressure that propagates through the domain.

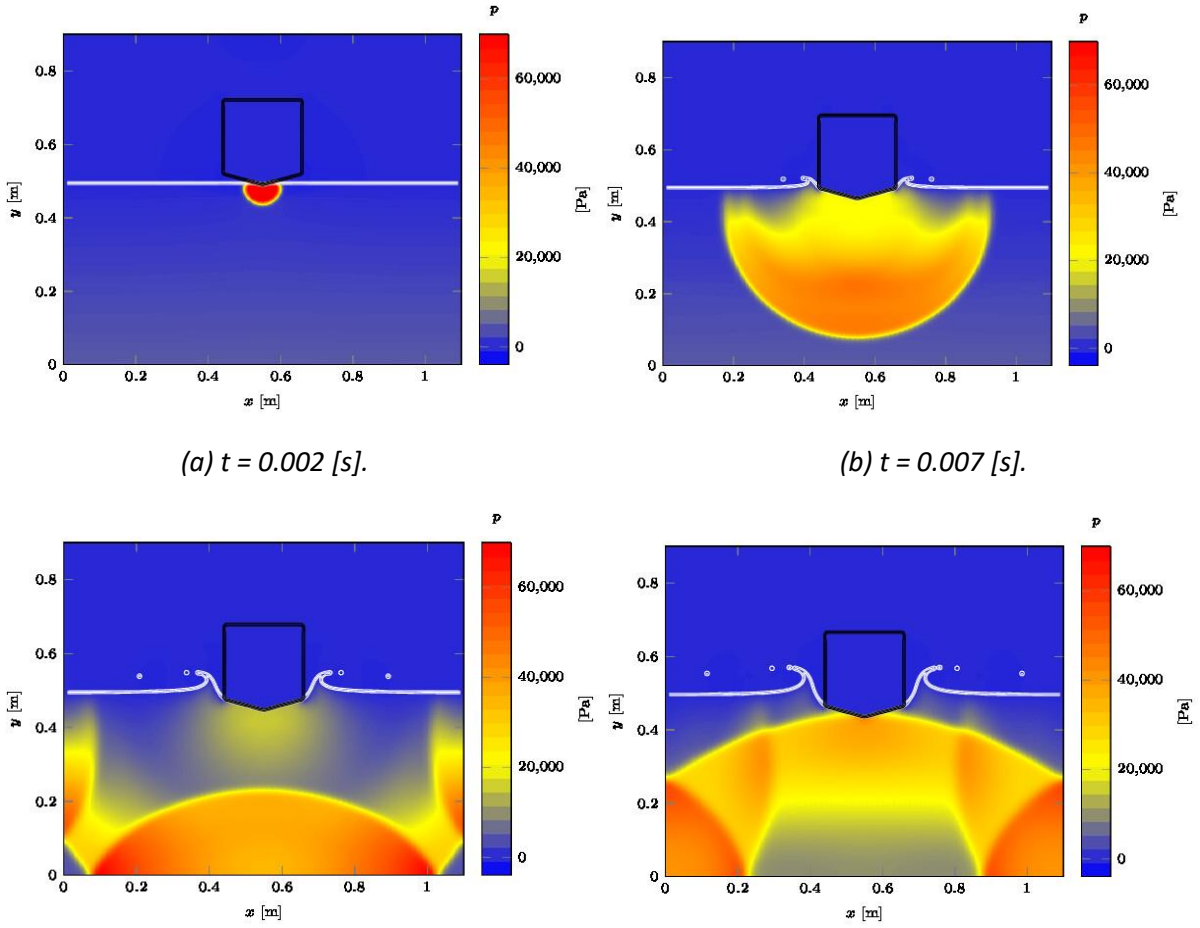

(a) t = 0.002 [s].

(b) t = 0.007 [s].

(c) t = 0.011 [s].

(d) t = 0.014 [s].

Figure 7. Time sequence of simulated pressure fields for wedge impact α = 15 [deg] and β_g = 0.04 [-] at different time instances. From the sequence it becomes apparent that density waves are formed that propagate through the domain.

Conclusion and future outlook

A new compressible pressure-based multiphase model is presented for modeling the interaction of homogeneous aerated water with moving bodies. The formulation was designed with efficiency in mind: it solves a system of equations that is no larger than the number of cells in the domain and it does not require iteration within a time step. The model can deal with high-density ratio compressible flows using a non-conservative formulation for transport of the interface together with a new formulation for the speed of sound in multiphase mixtures.

The numerical results are in good agreement with solutions for traditional compressible multiphase flow cases, such as a cylindrical helium shock bubble. The test cases demonstrate the method's ability to handle contact discontinuities and rarefactions. The pressure levels in propagating density waves

were predicted well, but the discontinuity between pressure levels was diffused over a couple of grid cells.

A 2D experimental setup for wedge impacts with water was converted specifically for this study to validate the numerical method for the interaction between aerated water and moving bodies in terms of the impact pressure. A level of 1% aeration by volume reduces the impact pressure by 14%. The numerical and experimental results are in good agreement for lower aeration levels, both showing a similar maximum pressure and development of the pressure over time. The differences at higher aeration levels are larger. We believe this to be due to three dimensional effects of the bubbles in the mixture in the experiment at higher aeration levels. These are not yet accounted for by the numerical method.

Future work will focus on representing the effects at higher aeration levels, both by means of numerical method development and new experiments to measure the distribution of gas bubbles in water.

References

Bredmose, H. Peregrine, D.H., and G.N. Bullock, G.N. (2009). Violent breaking wave impacts. part 2: modelling the effect of air. Journal of Fluid Mechanics, 641:389–430, 2009.

Haas, J.-F., Sturtevant, B. (1987). Interaction of weak shock waves with cylindrical and spherical gas inhomogeneities. Journal of Fluid Mechanics, 181:41–76.

Kreeft, J.J., Koren, B. (2010). A new formulation of kapila's five-equation model for compressible twofluid flow, and its numerical treatment. Journal of Computational Physics, 229(18):6220–6242.

Ma, Z.H., Causon, D.M., Qian L., Mingham, Mai, T., Greaves, D., Raby, A. (2016). Pure and aerated water entry of a flat plate. Physics of Fluids, 28(1):016104.

Plumerault, L.-R., Astruc, D., Maron, P. (2012). The influence of air on the impact of a plunging breaking wave on a vertical wall using a multifluid model. Coastal engineering, 62:62–74.

Quirk, J.J., Karni, S. (1996). On the dynamics of a shock–bubble interaction. Journal of Fluid Mechanics, 318:129–163.

van der Eijk, M. (2023). Extreme aerated water-wave impacts on floating bodies, PhD Thesis, Delft University of Technology.

van der Eijk, M., Wellens, P.R. (2019). A compressible two-phase flow model for pressure oscillations in air entrapments following green water impact events on ships. International Shipbuilding Progress, 66(4):315–343.

van der Eijk, M., Wellens, P.R. (2023). Two-phase free-surface flow interaction with moving bodies using a consistent, momentum preserving method. Journal of Computational Physics, 474:111796.

van der Eijk, M., Wellens, P.R. (2024). An efficient 2D bilinear interface reconstruction algorithm and consistent multidimensional unsplit advection scheme for accurate tracking of highly-curved interfacial structures on structured grids. Journal of Computational Physics, 498:112656.

Wood, A.B. (1941). A textbook of sound, 578 pp. Bell, London, 1941.